Scientific Reports

https://doi.org/10.1038/s41598-026-55539-0

Article in Press

Advanced hierarchical ZnFe-LDH@MnO_2 nanostructures for sensitive voltammetric determination of lenalidomide

Received: 27 March 2026

Accepted: 25 May 2026

Published online: 29 June 2026

Cite this article as: Özata Ç.A., Erk N., Özalp Ö. *et al.* Advanced hierarchical ZnFe-LDH@MnO_2 nanostructures for sensitive voltammetric determination of lenalidomide. *Sci Rep* (2026). https://doi.org/10.1038/s41598-026-55539-0

Çiğdem Aybüke Özata, Nevin Erk, Özgür Özalp & Mustafa Soylak

We are providing an unedited version of this manuscript to give early access to its findings. Before final publication, the manuscript will undergo further editing. Please note there may be errors present which affect the content, and all legal disclaimers apply.

If this paper is publishing under a Transparent Peer Review model then Peer Review reports will publish with the final article.

ARTICLE IN PRESS

© The Author(s) 2026. **Open Access** This article is licensed under a Creative Commons Attribution-NonCommercial-NoDerivatives 4.0 International License, which permits any non-commercial use, sharing, distribution and reproduction in any medium or format, as long as you give appropriate credit to the original author(s) and the source, provide a link to the Creative Commons licence, and indicate if you modified the licensed material. You do not have permission under this licence to share adapted material derived from this article or parts of it. The images or other third party material in this article are included in the article's Creative Commons licence, unless indicated otherwise in a credit line to the material. If material is not included in the article's Creative Commons licence and your intended use is not permitted by statutory regulation or exceeds the permitted use, you will need to obtain permission directly from the copyright holder. To view a copy of this licence, visit http://creativecommons.org/licenses/by-nc-nd/4.0/.

ARTICLE IN PRESS

Advanced Hierarchical ZnFe-LDH@MnO_2 Nanostructures for Sensitive Voltammetric Determination of Lenalidomide

Çiğdem Aybüke Özata[a,b*], Nevin Erk[a*], Özgür Özalp[c], and Mustafa Soylak [c, d,e]

[a] Ankara University, Faculty of Pharmacy, Department of Analytical Chemistry, 06560 Ankara, Türkiye.

[b] Ankara University, The Graduate School of the Health Sciences, 06110 Ankara, Türkiye.

[c] Erciyes University, Faculty of Sciences, Department of Chemistry, 38039, Kayseri, Türkiye.

[d] Technology Research & Application Center (TAUM), Erciyes University, 38039, Kayseri, Türkiye.

[e] Turkish Academy of Sciences (TUBA), Cankaya, Ankara, Türkiye.

ARTICLE IN PRESS

Emails of the corresponding authors: erk@pharmacy.ankara.edu.tr

caozata@ankara.edu.tr

ARTICLE IN PRESS

Abstract

The accurate determination of lenalidomide (LEN) is essential due to its widespread clinical use and narrow therapeutic window. In this context, a novel, eco-friendly electrochemical sensor based on a ZnFe-LDH@MnO_2 nanocomposite-modified glassy carbon electrode (ZnFe-LDH@MnO_2/GCE) was developed for the sensitive determination of LEN. The hybrid nanocomposite was synthesized via a rapid two-step procedure involving microwave-assisted formation of ZnFe-LDH followed by controlled MnO_2 deposition. Structural and physicochemical characterization using Fourier-transform infrared spectroscopy (FTIR), X-ray diffraction (XRD) analysis, Field emission scanning electron microscopy/Energy dispersive X-ray spectroscopy (FE-SEM/EDX), Brunauer-Emmet-Teller (BET) analysis, and Thermogravimetric analysis (TGA) confirmed the successful formation of a hierarchically structured nanocomposite with a significantly increased surface area (113.88 m^2/g for ZnFe-LDH@MnO_2 vs. 77.40 m^2/g for ZnFe-LDH) and improved thermal stability. Electrochemical studies revealed enhanced electron-transfer kinetics, evidenced by a decrease in charge-transfer resistance (Rct) from 3218.7 Ω to 1050.1 Ω and an increase in electroactive surface area from 0.085 cm^2 to 0.14 cm^2 after modification.

LEN exhibited an irreversible oxidation process involving a $2e^-/1H^+$ mechanism, which was quantitatively monitored using differential pulse voltammetry (DPV). Under optimized conditions, the sensor demonstrated a wide linear range of 0.50–9.80 µM (R^2 = 0.995), with a low limit of detection (LOD) of 6.99 nM. The developed platform showed excellent repeatability (relative standard deviation, RSD = 1.1%) and reproducibility (RSD = 0.4%), along with high selectivity against common interfering species.

Furthermore, the environmental impact of the method was evaluated using Green Analytical Procedure Index (GAPI), Analytical GREEnness (AGREE) (0.84), and Blue Applicability Grade Index (BAGI) (77.5) tools, confirming its sustainability and practical applicability. The sensor was successfully applied to human plasma, synthetic urine, and pharmaceutical dosage forms, yielding satisfactory recoveries (98.2%–101.7%). These results demonstrate that the proposed sensor provides a green, sensitive, and cost-effective alternative for routine LEN determination in clinical and pharmaceutical analysis.

ARTICLE IN PRESS

ARTICLE IN PRESS

Keywords

Biological samples; Differential pulse voltammetry; Lenalidomide; Pharmaceutical analysis; ZnFe-LDH@MnO_2-modified glassy carbon electrode

1. Introduction

Multiple myeloma (MM) is a malignant plasma cell disorder characterized by uncontrolled proliferation of abnormal plasma cells within the bone marrow, leading to bone destruction, anemia, renal impairment, and immunodeficiency [1]. In recent decades, lenalidomide (LEN), a potent immunomodulatory analog of thalidomide, has revolutionized the management of MM [2]. Due to its narrow therapeutic window and its indispensable role in long-term maintenance therapy, the accurate determination of LEN in pharmaceutical and biological matrices is critical for ensuring patient safety and dosage precision [3].

Several analytical techniques have been developed for the quantitative determination of LEN in pharmaceutical formulations and biological matrices to ensure its accurate dosage and therapeutic monitoring. These include high-performance liquid chromatography coupled with mass spectrometry (HPLC–MS/MS) [4], ultra-performance liquid chromatography with tandem mass spectrometry (UPLC–MS/MS) [5], liquid chromatography with tandem mass spectrometry (LC-MS/MS) [6-8], fluorimetric and UV–visible spectrophotometric methods [9], as well as various reversed-phase HPLC (RP-HPLC) assays [10,11]. Additionally, non-extractive HPLC procedures using fluorescence detection after pre-column derivatization with fluorescamine [12], and capillary electrophoresis methods equipped with photodiode array detection [13], have also been reported. Although these methods offer excellent sensitivity and accuracy, they are often limited by labor-intensive sample preparation, high operational costs, and prolonged analysis times. These drawbacks create a clear demand for analytical strategies that are simpler, faster, and more affordable [14-16].

In this regard, electrochemical methods offer a promising alternative owing to their high sensitivity, low cost, rapid analysis, and minimal sample preparation. Particularly, techniques such as DPV are highly valued for their ability to provide superior sensitivity and low detection limits while significantly reducing analysis time. The effectiveness of these techniques is further enhanced by the selection of the glassy carbon electrode (GCE) as the primary transducer. The GCE is widely preferred due to its broad operational potential window, excellent electrical conductivity, and high chemical inertness, which ensures low background currents and improved signal-to-noise ratios [17]. Furthermore, the GCE's robust surface is uniquely suited for stable modification with advanced nanomaterials, facilitating the development of highly efficient and reproducible sensing interfaces. These advantages are consistent with modern trends in analytical chemistry aimed at creating sustainable and high-performance sensing platforms [18,19]. Additionally, surface modification of electrodes with nanocomposite materials enhances

ARTICLE IN PRESS

selectivity and detection limits, making electrochemical sensing a green and efficient approach for LEN determination [20].

Layered double hydroxides (LDHs) have emerged as highly attractive electrode materials for electrochemical sensing due to their unique two-dimensional lamellar structure, high specific surface area, and tunable chemical composition [21-24]. Among the various combinations, ZnFe-LDH is particularly notable for its biocompatibility, low toxicity, and cost-effectiveness [25]. The coexistence of mixed-valence iron and zinc ions within the brucite-like layers coordinates highly dense, electrocatalytic active centers for the oxidation reaction, while the defined interstitial channels accelerate the mass transport and intra-crystalline diffusion of the analyte [23,26]. However, pristine LDHs often suffer from limited electrical conductivity and the tendency of nanosheets to aggregate due to van der Waals forces, which can hinder their full electrochemical potential. It is now clear what kind of interlayer anion is present in the ZnFe-LDH structure. The interlayer anion was found to be CO_3^{2-}, which is compatible with the FTIR/XRD results, taking into account the use of NaOH and Na_2CO_3 during synthesis. The purpose of adding this information is to make the material's layered structure easier to comprehend [27].

To overcome these limitations and further enhance the sensing performance, the incorporation of transition metal oxides, such as manganese dioxide (MnO_2), is an effective strategy. MnO_2 is widely valued in electrochemistry for its excellent catalytic activity, natural abundance, and environmental friendliness [28,29]. When deposited onto the LDH surface, MnO_2 nanostructures not only improve the electrical conductivity of the nanocomposite but also act as spacers to prevent the restacking of LDH layers [30]. This synergistic combination results in a hierarchical heterostructure with an enlarged electroactive surface area and enhanced electron transfer rates, thereby significantly improving the sensitivity and selectivity of the sensor for the detection of pharmaceutical compounds [31,32].

To the best of our knowledge, this work presents the first application of a hierarchically structured ZnFe-LDH@MnO_2 nanocomposite for the sensitive voltammetric determination of LEN. The novelty of this approach lies in the synergistic integration of microwave-assisted ZnFe-LDH synthesis with controlled MnO_2 deposition. This rapid two-step procedure results in a significant expansion of the electroactive surface area and enhanced electron-transfer kinetics compared to unmodified surfaces, facilitating a sensitive $2e^-/1H^+$ oxidation process.

Furthermore, this study bridges the gap between high-performance sensing and sustainability, offering a rapid, cost-effective alternative to traditional, labor-intensive chromatographic methods. The method's unique contribution is quantitatively verified by modern greenness assessment tools, achieving high sustainability scores of 0.84 (AGREE) and 77.5 (BAGI), thereby providing a robust and environmentally conscious platform for routine clinical and pharmaceutical analysis.

ARTICLE IN PRESS

2. Methodology

2.1. Chemicals, Reagents, and Materials

The specifications and sources of the chemicals and reagents used are listed in the Supporting Information (SI).

2.2. Instruments

Details of the instruments used are provided in the SI.

2.3. Synthesis of the Nanocomposite

2.3.1. Synthesis of ZnFe-LDH

1.5 M $ZnCl_2$ (10.2 g), 0.5 M $FeCl_3.6H_2O$ (6.76 g), 0.35 M NaOH (0.8 g), and 0.15 M Na_2CO_3 (0.7 g) were weighed and placed in a beaker. 20 mL of deionized water was added and stirred on a magnetic stirrer (room temperature) for 1 hour. The reaction was then conducted in a microwave oven at 300 W and 150°C for 30 minutes. The slurry obtained after centrifugation was washed twice with distilled water and ethanol and dried in a 60°C oven [33].

2.3.2. Synthesis of ZnFe-LDH@MnO_2

0.3 g of the synthesized ZnFe-LDH material was added to 50 mL of distilled water and 0.05 g of $MnCl_2.4H_2O$. The mixture was stirred for 1 hour on a magnetic stirrer (at room temperature). 0.06 g of KMnO4 was then added, and stirring continued for another 6 hours. The resulting slurry was washed three times with distilled water and ethanol, and dried in a 60°C oven.

2.4. Fabrication of the ZnFe-LDH@MnO_2/GCE

The modification procedure of the GCE was carried out using the nanocomposite material denoted as ZnFe-LDH@MnO_2. Initially, a specific amount of ZnFe-LDH@MnO_2 powder was transferred into a microtube, and distilled water was added to prepare a homogeneous dispersion. The mixture was vortexed for approximately 5 min, followed by ultrasonication for 15 min to ensure complete dissolution and uniform dispersion of the nanocomposite. The resulting suspension was used as the stock solution for electrode modification.

Prior to modification, the bare GCE surface was carefully polished with an alumina slurry on a polishing pad for 5 minutes to achieve a mirror-like finish. The electrode was then rinsed and placed in a beaker containing a 1:1 (v/v) ethanol–water mixture and sonicated for 5 min to remove any residual polishing material. Afterward, the electrode was washed thoroughly with distilled water and allowed to dry at room temperature.

Finally, based on the optimized modification parameters determined in the optimization studies, a specific volume of the prepared ZnFe-LDH@MnO_2 suspension was drop-cast onto the conductive

ARTICLE IN PRESS

surface of the cleaned GCE. The ZnFe-LDH@MnO_2/GCE was then left to dry under UV light to ensure proper adhesion and solvent evaporation, yielding the ZnFe-LDH@MnO_2/GCE ready for subsequent electrochemical measurements.

2.5. Spiked Samples

To evaluate the applicability of the developed electrochemical method in real matrices, analyses were performed using pharmaceutical dosage form, human plasma, and synthetic urine samples.

Human plasma: For plasma sample preparation, equal volumes of human plasma and acetonitrile (1:1, v/v) were mixed to precipitate plasma proteins [34]. The mixture was centrifuged at 8000 rpm for 20 min, and the clear supernatant was carefully collected without disturbing the precipitate. The obtained supernatant was then spiked with the standard LEN solution to achieve the desired concentrations, based on the calculated amounts.

Synthetic urine: To avoid ethical concerns associated with human sample collection, a synthetic urine solution was prepared to simulate the composition of real urine [35]. The artificial matrix was prepared by incorporating essential physiological constituents, including potassium chloride (KCl), sodium phosphate (Na_3PO_4), sodium sulfate (Na_2SO_4), uric acid ($C_5H_4N_4O_3$), and glucose ($C_6H_{12}O_6$), to simulate the ionic strength and chemical complexity of human urine. Prior to spiking, the synthetic urine was filtered through a 0.45 µm PTFE membrane filter to remove any particulate matter and ensure clarity. The filtered solution was then spiked with the LEN standard solution to obtain the required concentrations according to the calculated volumes, and subsequently subjected to electrochemical measurements under identical conditions.

Pharmaceutical dosage form: Three commercial capsules containing LEN were accurately weighed after carefully removing their powdered contents composed of the active ingredient and excipients. Based on the obtained average weight and drug label information, an appropriate portion corresponding to the desired concentration was calculated and transferred into a volumetric flask. The sample was then dissolved in a 1:1 (v/v) ethanol–water mixture and diluted to the target concentration for electrochemical analysis.

3. Results and Discussion

3.1. Characterization of the Nanocomposite

Fourier-transform infrared spectroscopy (FTIR) analysis

FTIR spectra of the Zn–Fe LDH@MnO_2 nanocomposite and its constituents are shown in Figure S1. The peaks at 3435 and 3485 cm^{-1} represent the stretching vibrations of hydroxyl groups (-OH). The bands at 1510 and 1780 cm^{-1} represent the vibrations of C-O and C-C groups, respectively [36]. The bands in the 400 to 900 cm^{-1} region correspond to M-O and O-M-O, while the peaks at 639, 830, and 990 cm^{-}

ARTICLE IN PRESS

[1] originate from the O-M-O, M-O-M, and M-O stretching vibrations in the Zn–Fe LDH@MnO_2 nanocomposite, respectively [37,38]. In particular, peak shifts and intensity changes are highlighted as proof of interfacial interactions within the composite, and the discussion now links the observed bands with structural characteristics of both Zn–Fe LDH and MnO_2. The absorption bands in the fingerprint region (400–1000 cm^{-1}) were attributed to metal–oxygen vibrations: bands at 490–530 cm^{-1}, 580–630 cm^{-1}, and 720–780 cm^{-1} correspond to Zn–O, Fe–O, and Mn–O stretching modes, respectively. Additionally, the band at 750–820 cm^{-1} was assigned to Mn–O–Mn vibrations. These results confirm the successful formation and integration of the metal oxide framework in the synthesized material. The materials production and physicochemical characteristics are better understood as a result of these improvements.

X-ray diffraction analysis

The ZnFe-LDH and ZnFe-LDH@ MnO_2 nanocomposites powder X-ray diffraction (XRD) patterns (Bruker AXS D8 Advanced diffractometer) are shown in Figure S2. Four noticeable diffraction peaks, corresponding to the (110), (200), (002), and (211) crystallographic planes, are visible in the ZnFe-LDH @MnO_2 sample at 2θ = 12.8°, 18.7°, 27.3°, and 36.7°. These reflections show that the hybrid material was successfully formed and are typical of layered or nanocomposite structures including MnO_2 [39-41].

Additionally, the primary diffraction peaks associated with the parent ZnFe-LDH phase are retained in the ZnFe-LDH@ MnO_2 nanocomposite, appearing at almost identical 2θ positions but with significantly lower intensities. This decrease in peak intensity shows that the fundamental layered double hydroxide framework is still there in the nanocomposite, but it also suggests that MnO_2 deposition may have partially changed the structure. The successful development of the LDH structure is confirmed by the reflections at 2θ = 12.8°, 18.7°, 27.3°, and 36.7°, which match its distinctive basal planes. Because of its low concentration, significant dispersion within the LDH matrix, and/or amorphous or weakly crystalline character, there are no clear MnO_2 peaks in the XRD pattern. Consequently, a widely dispersed and low-crystallinity phase is suggested rather than its absence by the lack of visible MnO_2 peaks [40-42].

A valid estimate of crystallite size using the Scherrer equation was not possible because of the broad and overlapping diffraction peaks seen in the XRD patterns, which are linked to the low crystallinity and nanoscale dispersion of the metal oxide phases. As a result, complementary methods like SEM and TEM investigations were mostly used to assess the structural characteristics of the manufactured materials.

Morphological and Elemental Analysis

As seen in Figure 1, respectively, the morphological features and particle diameters of the produced ZnFe-LDH and ZnFe-LDH@MnO_2 nanomaterials were examined using scanning electron microscopy (SEM) (ZEISS Gemini 550, Germany). Image ProPlus 6.0 was used to calibrate and assess the scale

ARTICLE IN PRESS

bars, which showed particle sizes between 40 and 1000 nm. In addition to the morphological evaluation, elemental mapping and SEM in conjunction with EDX were carried out to clarify the elemental distribution in both materials (Figures 2 and 3).

The MnO_2-modified nanocomposite and the pure ZnFe-LDH exhibit distinct morphological differences in the FE-SEM pictures. The lamellar and platelet-like nanosheets that make up ZnFe-LDH are unevenly stacked and collected into dense clusters, giving it the distinctive appearance of layered double hydroxides [43,44]. The intrinsic layered nature of LDH structures, which usually results from fast nucleation followed by spontaneous sheet stacking and aggregation a phenomenon frequently documented for Zn- and Fe-based LDHs-is reflected in the somewhat folded and crumpled edges of these sheets.

There is a noticeable change in surface morphology after MnO_2 deposition. MnO_2 nanocomposites domains uniformly adorn the previously smooth LDH lamellae, giving them a coarser, more granular surface texture. LDH nanosheets coated with MnO_2 nanostructures provide a hierarchical structural arrangement that adds several nanoscale asperities and improves surface heterogeneity [45]. This morphological progression is in line with studies in the literature on LDH–MnO_2 hybrid systems, where the successful creation of the ZnFe-LDH@MnO_2 nanocomposite is confirmed and surface activity is efficiently increased by MnO_2 nucleation on LDH surfaces.

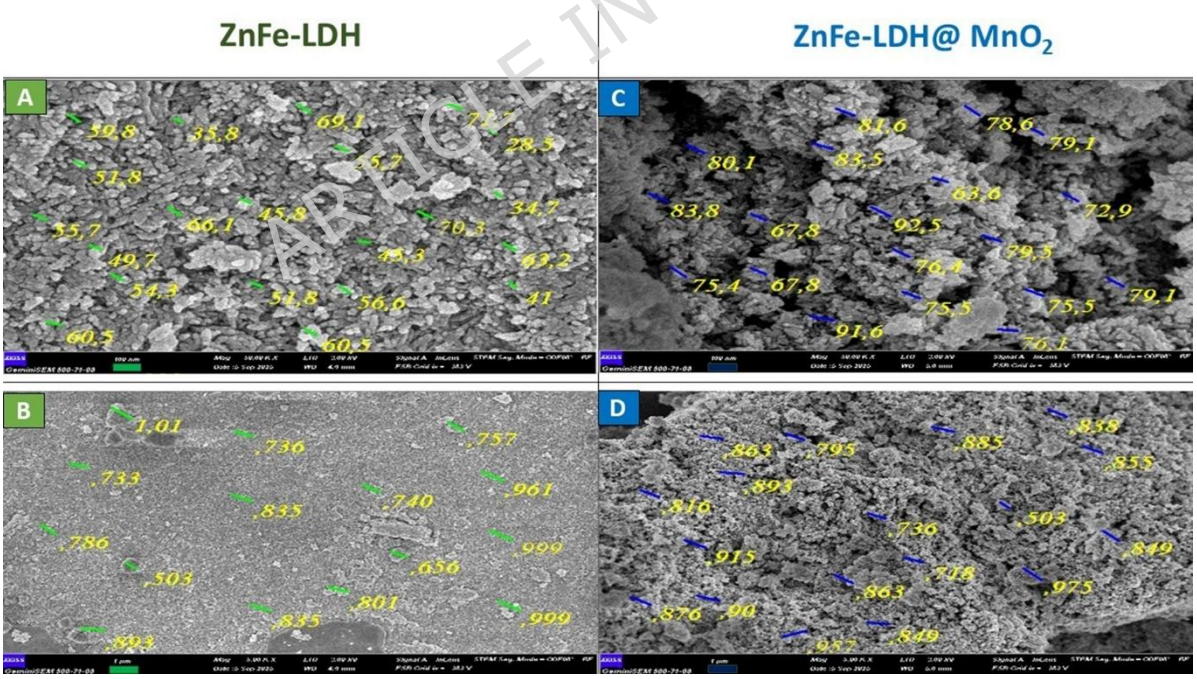


Figure 1. SEM images ZnFe-LDH, and ZnFe-LDH@MnO_2 (A and C :100 nm, 50kx, B and D: 1 µm, 5.0 kx)

The surface chemical composition of the synthesized ZnFe-LDH was examined by EDX analysis (Figure 2). The elemental distribution revealed the presence of C, N, O, Cl, Fe, and Zn at 9.57%, 1.95%,

ARTICLE IN PRESS

30.58%, 9.94%, 46.43%, and 1.54%, respectively, which is consistent with the expected elemental framework of the layered double hydroxide.

Following the surface modification of ZnFe-LDH with MnO_2, the EDX spectrum showed notable changes in elemental composition (Figure 3). The coated material, ZnFe (LDH)@MnO_2, contained C, N, O, Cl, Mn, Fe, and Zn at 10.18%, 2.16%, 39.07%, 3.29%, 19.90%, 25.28%, and 0.12%, respectively. The significant increase in Mn content, accompanied by a corresponding shift in Fe and O proportions, confirms the successful MnO_2 deposition onto the ZnFe (LDH) surface, in agreement with the FESEM, FTIR and XRD results.

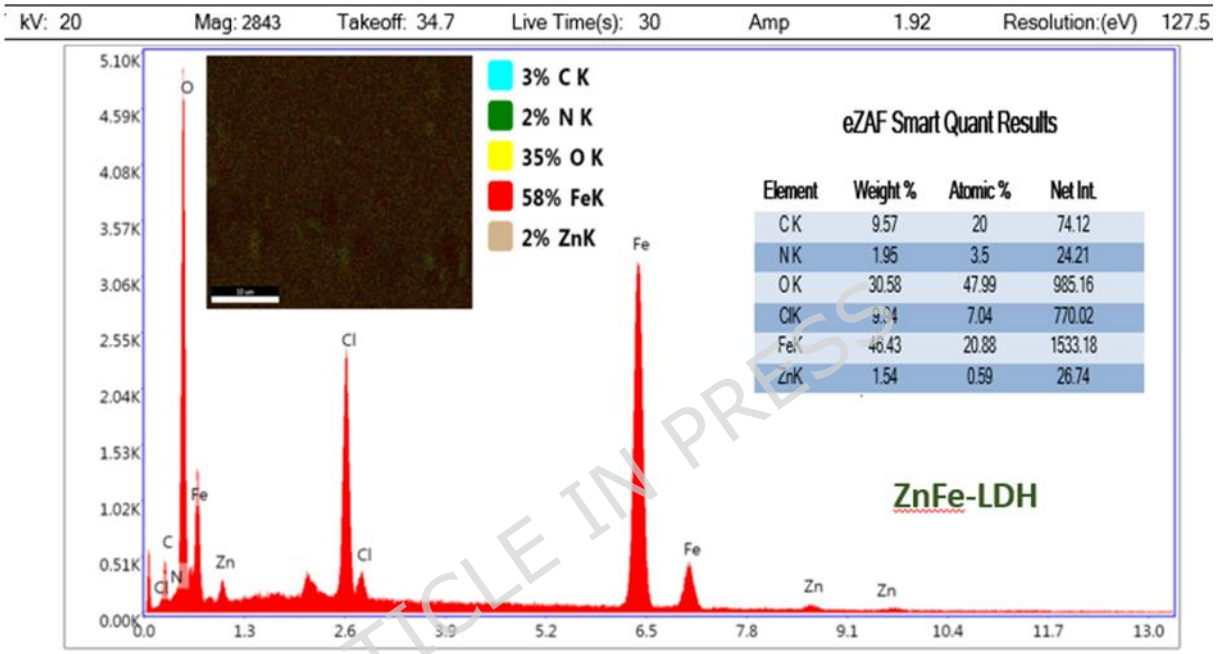
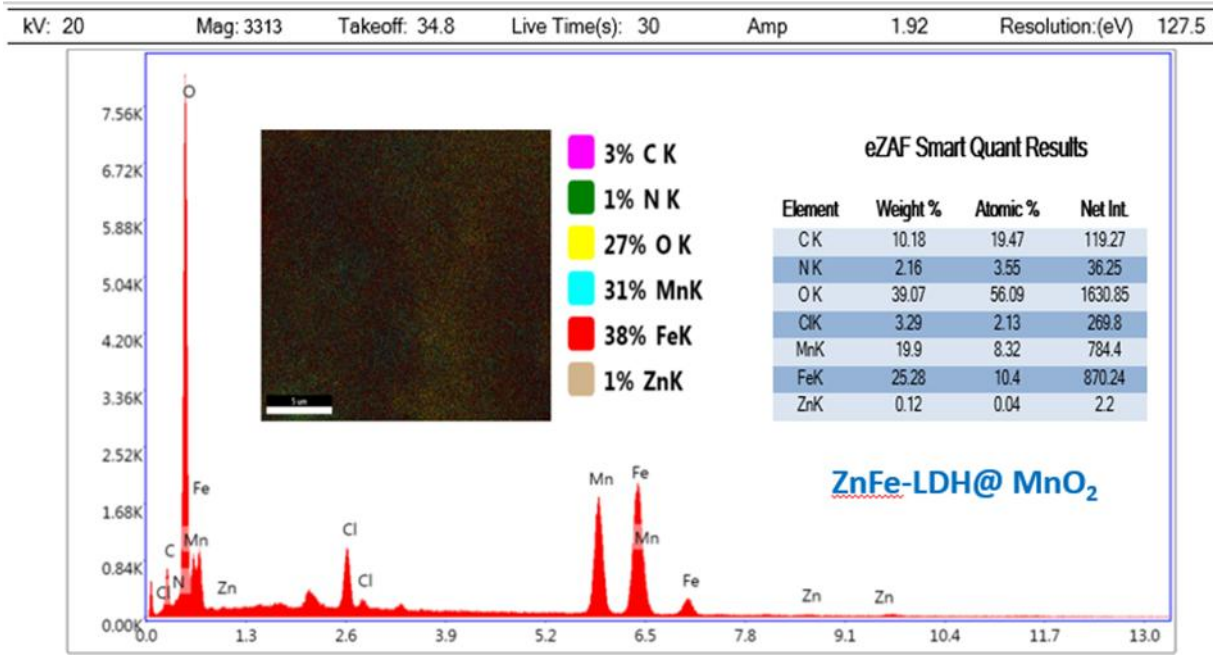


Figure 2. SEM-EDX and Mapping analysis for ZnFe-LDH



ARTICLE IN PRESS

Figure 3. SEM-EDX and Mapping analysis for ZnFe-LDH@MnO_2

Brunauer-Emmet-Teller (BET) analysis

BET measurements were performed using a Micromeritics Gemini VII and Tristar II Plus systems to evaluate the surface characteristics of the powder nanocomposites (Figure 4). The ZnFe-LDH sample displayed a BET specific surface area of 77.4068 m^2/g. Its pore structure, assessed through BJH analysis, showed average adsorption and desorption pore widths of 85.951 Å and 68.513 Å, respectively.

Following MnO_2 modification, the ZnFe-LDH@MnO_2 nanocomposite exhibited a pronounced increase in BET surface area, reaching 113.8862 m^2/g. The BJH adsorption and desorption pore widths also expanded to 164.973 Å and 141.463 Å, indicating a notable enlargement of pore dimensions after coating.

Overall, the MnO_2 deposition significantly enhanced the accessible surface and broadened the pore structure of the powder nanocomposite, suggesting that the coating process effectively generated a more open and surface-active architecture (Figure 4).

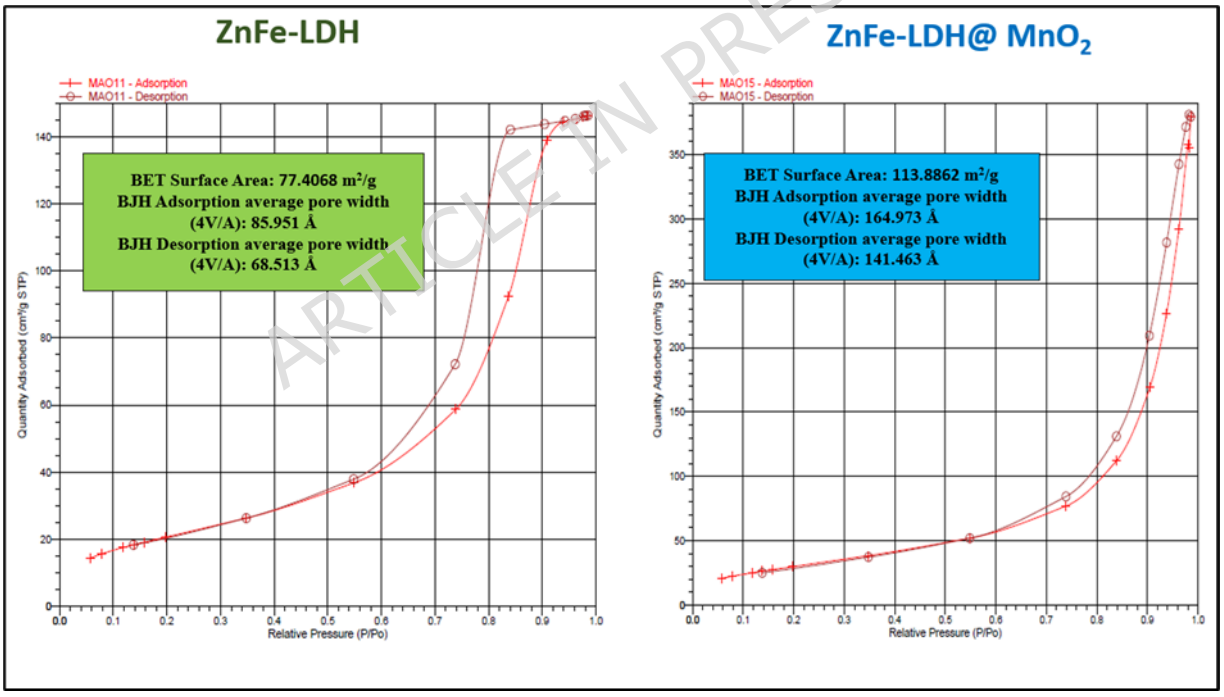


Figure 4. BET analysis of ZnFe-LDH, and ZnFe-LDH@MnO_2 nanocomposite.

Thermogravimetric analysis

Two significant weight-loss events, occurring at roughly 150 °C and 430 °C, respectively, are shown by thermogravimetric analysis (TGA) of the materials. According to the well-established dehydration behavior of layered double hydroxides (LDHs), the initial mass loss at 150 °C is usually ascribed to the

ARTICLE IN PRESS

removal of physisorbed and interlayer water molecules. The dehydroxylation of the brucite-like layers and the ensuing collapse of the LDH structure, a typical thermal transition frequently documented for Zn–Fe-based LDHs, correspond to the second notable deterioration step around 430 °C. The ZnFe-LDH@MnO_2 nanocomposite shows (Figure S3) a somewhat altered and less noticeable thermal degradation profile as comparison to the pristine ZnFe-LDH. The MnO_2-modified LDH exhibits better thermal stability, as seen by its more gradual mass-loss progression and the delayed structural collapse, even though both materials decompose within a comparable temperature range [46]. This increase in heat resistance is in line with earlier findings that MnO_2 inclusion strengthens the structural rigidity of LDH frameworks by producing a more robust hybrid architecture and adding more metal-oxygen connections [47].

Overall, the TGA results support the successful development of a thermally more resilient nanocomposite material by confirming that ZnFe-LDH@MnO_2 has better thermal stability than the unmodified ZnFe-LDH, which is consistent with findings in the literature.

3.2. Determination of PZC

As shown in Figure S4, the ZnFe-LDH@MnO_2 nanocomposites point of zero charge (PZC) was found utilizing the pH drift method within an initial pH range of 3–12. Throughout the acidic to near-neutral area, the ΔpH readings stayed near zero and slightly positive. At an initial pH of roughly 6.3, the ΔpH curve crossed the zero line, revealing the materials PZC [48].

Because surface hydroxyl groups are protonated below this pH, the adsorbent surface has a net positive charge that promotes the adsorption of anionic species. On the other hand, ΔpH gradually turns negative at pH values higher than 6.3, indicating deprotonation and the formation of a negatively charged surface that improves the adsorption of cationic analytes. Partial dissolution or surface restructuring, which is commonly seen in LDH-based nanocomposite under alkaline circumstances, may be the cause of a modest increase in ΔpH at higher pH levels.

Overall, ZnFe-LDH@MnO_2's PZC was found to be roughly pH 6.3, indicating that, depending on the pH of the solution, the material can interact with either anionic or cationic medicinal analytes. For adsorption-based preconcentration of medicinal compounds, including anticancer medicines, whose ionization state changes with pH, this variable surface charge behavior is beneficial. It should be noted that certain surface chemistry effects, such as the presence of metal oxide functionalities and adsorbed ionic species, may cause the apparent deviation in the pH_pzc trend. Under certain experimental conditions, these effects can change the protonation–deprotonation behavior and result in atypical surface charge characteristics.

3.3. Electrochemical Behavior

To investigate the electron-transfer behavior at the electrode interface and assess the electrochemical properties of the modified surfaces, cyclic voltammetry (CV) and electrochemical impedance

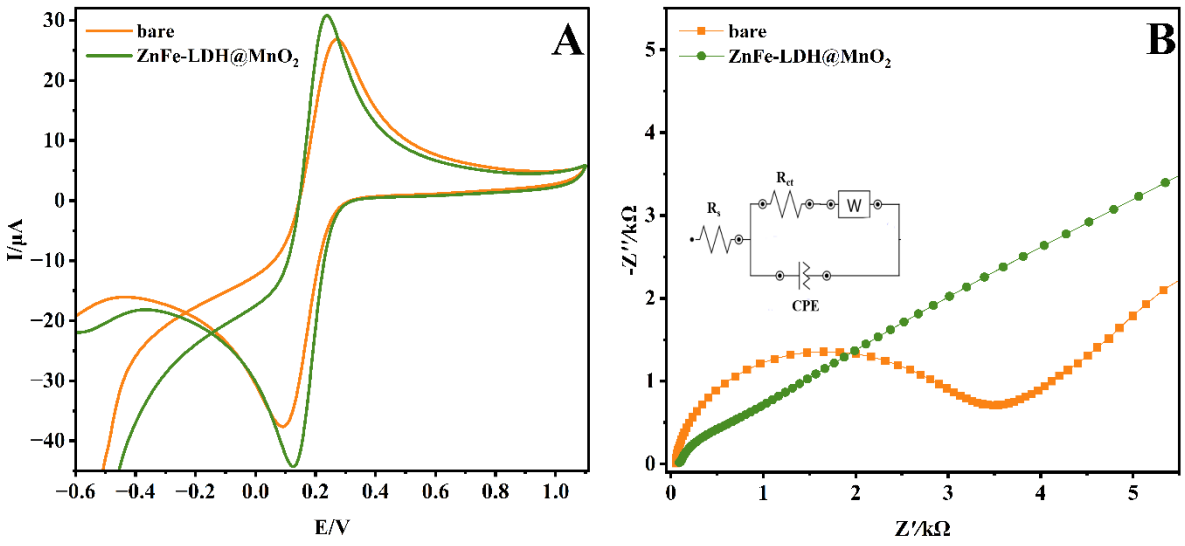
ARTICLE IN PRESS

spectroscopy (EIS) analyses were carried out using 5.0 mM $[Fe(CN)_6]^{3-/4-}$ in 0.1 M KCl as the redox indicator system.

The electrochemical responses of the bare electrode and ZnFe-LDH@MnO_2/GCE were first compared by CV at different scan rates ranging from 10 to 300 mV s^{-1} (Figure S5A-C). The electroactive surface areas (A) were calculated from the slopes of the I_p versus $\nu^{1/2}$ plots (Figure S5B-D) using the Randles–Ševčík equation (Equation S1), yielding 0.085 cm^2 for the bare electrode and 0.14 cm^2 for the modified one.

CVs obtained at a scan rate of 50 mV s^{-1} for both electrodes are presented in Figure 5A, demonstrating the basis for ΔE_p determination. The ZnFe-LDH@MnO_2/GCE exhibited a smaller peak-to-peak separation (ΔE_p = 0.10 V) compared to the bare electrode (ΔE_p = 0.17 V), suggesting an improvement in electron-transfer kinetics following surface modification. This observation indicates that the modification contributes to an increased electroactive area and facilitates charge transfer at the electrode–electrolyte interface, which may be associated with changes in surface morphology and conductivity arising from the nanocomposite structure.

EIS measurements were conducted to gain deeper insight into the charge-transfer processes of the bare and modified electrodes under the same electrolyte conditions. As shown in Figure 5B, the Nyquist plots exhibited a typical semicircular region at high frequencies corresponding to the charge-transfer resistance (Rct). The Rct value for the bare electrode was found to be 3218.7 Ω, whereas that of the ZnFe-LDH@MnO_2/GCE significantly decreased to 1050.1 Ω, indicating an improved electron transfer capability after modification. Based on the EIS data, the standard heterogeneous electron transfer rate constant (k^0) and the exchange current density (j^0) were also calculated (Equations S2 and S3). The k^0 values were determined as 1.94×10^{-4} cm s^{-1} for the bare electrode and 3.65×10^{-4} cm s^{-1} for the modified one, while the corresponding j^0 values were 7.98×10^{-6} A cm^{-2} and 24.5×10^{-6} A cm^{-2}, respectively.



ARTICLE IN PRESS

Figure 5. (A) CV curves and (B) EIS plots for both the unmodified electrode (a) and ZnFe-LDH@MnO_2/GCE (b) in a solution of $[Fe(CN)6]^{3-/4-}$ (5 mM) and KCl.

The electrochemical parameters obtained from both CV and EIS analyses are summarized in Table 1. These results collectively demonstrate that surface modification leads to enhanced electroactive area and improved charge-transfer characteristics, which can be attributed to the presence of the ZnFe-LDH@MnO_2 nanocomposite providing a more conductive and electrochemically accessible interface.

Table 1. CV and EIS analysis of electrochemical behavior across electrode types.

Electrode	**A (cm^2)**	**ΔE_p (V)**	**k^0 (cm s^{-1})**	**j_0 (A cm^{-2})**
Bare	0.085	0.17	1.94×10^{-4}	7.98×10^{-6}
ZnFe-LDH@MnO_2/GCE	0.14	0.1	3.65×10^{-4}	24.5×10^{-6}

3.4. Investigation of LEN by Voltammetry

To determine the most suitable voltammetric technique for the quantitative analysis of LEN, both CV and DPV were comparatively evaluated. Initially, CV measurements were performed using a 100 µM LEN solution after recording the blank, in which no signal was observed, confirming the absence of any background response. On the bare electrode, an anodic peak current of 0.425 µA was obtained, which increased to 0.696 µA after surface modification (Figure 6A). Although CV is instrumental for elucidating the redox mechanism, its sensitivity is inherently limited by the continuous presence of background charging current.

In contrast, DPV measurements were conducted under identical conditions yielded a significantly enhanced response While the blank remained clear, the bare electrode exhibited a peak current of 1.31 µA, whereas the ZnFe-LDH@MnO_2/GCE showed a pronounced increase to 2.56 µA (Figure 6B). The superiority of DPV in this study is attributed to its unique pulse waveform, which effectively discriminates the faradaic current from the non-faradaic (charging) current. By sampling the current specifically at the end of each pulse—where the capacitive charging current has significantly decayed—DPV provides a much higher signal-to-noise ratio and sharper, better-defined peaks compared to CV. This technical advantage was crucial for achieving the nanomolar detection limits required for pharmaceutical and clinical monitoring [49]. Consequently, due to its exceptional sensitivity and ability to provide a clean analytical signal in complex matrices, DPV was selected as the optimal technique for all subsequent quantitative analyses.

ARTICLE IN PRESS

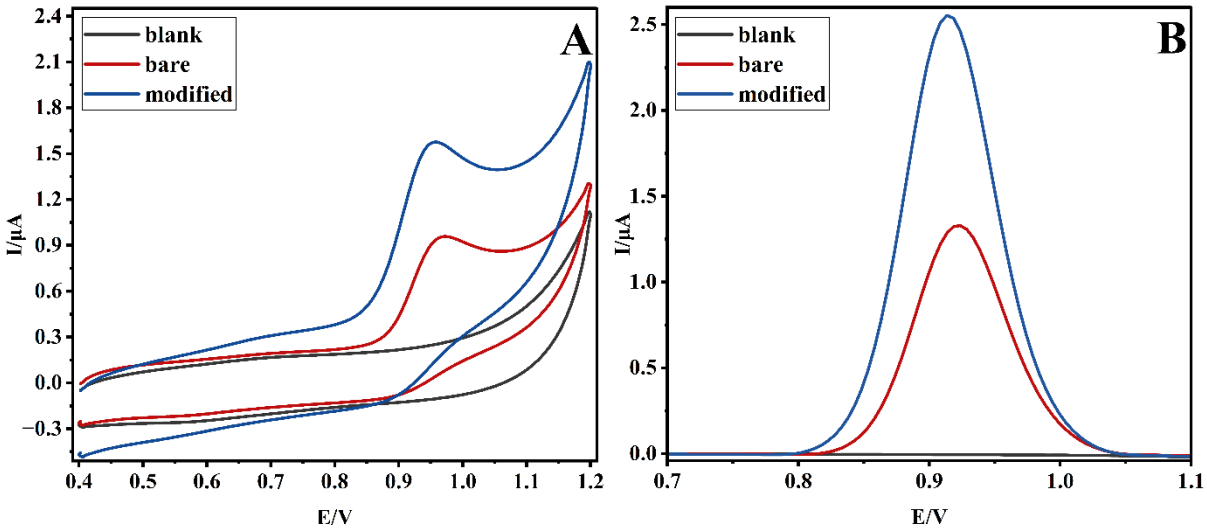


Figure 6. DPV (A) and CV (B) responses of BR (0.1 M, pH = 4.0) in the absence and presence of 100 μM LEN at the surface of unmodified GCE and ZnFe-LDH@MnO_2/GCE.

3.5. Optimization of Analytical Parameters

In the initial stage of optimization, the influence of the electrolyte medium on the electrochemical behavior of 100 μM LEN was examined at the ZnFe-LDH@MnO_2/GCE surface. For this purpose, four different supporting solutions were tested under identical conditions: 0.1 M BR buffer (pH 2.0), 0.1 M PBS (pH 2.0), 0.1 M HCl, and 0.1 M NaOH (Figure S6). The results indicated that the oxidation current of LEN significantly varied depending on the electrolyte, with the BR buffer providing the most favorable analytical response.

In the subsequent step of the optimization studies, the influence of the nanocomposite modifier concentration and its applied volume on the electrochemical response of LEN was systematically investigated. Different concentrations (0.5, 1.0, 1.5 and 2.0 μM) and deposition volumes (2.0, 3.0, 4.0, 5.0, 6.0, 7.0 and 8.0 μL) of the nanocomposite suspension were tested to achieve the highest oxidation peak current and the most stable signal. As presented in Figure S7A, the effect of the applied nanocomposite volume on the electrode surface was evaluated, and the optimal volume was determined based on the maximum and most reproducible current response. Nanocomposite concentration was also tested, as can be seen in the Figure S7B, the LEN oxidation current initially increased with increasing nanocomposite concentration up to an optimal value, after a decrease was observed, likely due to surface saturation and hindered electron transfer. These findings confirm that careful control of both nanocomposite concentration and loading volume is crucial for achieving optimal electrochemical performance of the ZnFe-LDH@MnO_2/GCE. As a result of these investigations, a nanocomposite concentration of 1 M and an applied volume of 6 μL were selected as the optimal conditions for further electrochemical experiments.

ARTICLE IN PRESS

To optimize the experimental parameters for the electrochemical detection of LEN, the effect of pH on its voltammetric behavior was investigated. For this assessment, BR buffer solutions covering a pH range of 2.0–9.0 were utilized. As shown in Figure 7A, the oxidation peak current of LEN increased gradually with increasing pH and reached its maximum intensity at pH 4.0. Beyond this point, a marked decrease in peak current was observed, suggesting that highly acidic or alkaline media are less favorable for LEN oxidation. Therefore, pH 4.0 was selected as the optimal condition for subsequent electrochemical measurements to ensure maximum sensitivity.

In addition, the dependence of the oxidation peak potential (Ep) on pH exhibited a linear relationship, as illustrated in Figure 7B. The slope of the obtained line was −0.024 V per pH unit, which is approximately half of the theoretical Nernstian value of −0.059 V/pH corresponding to equal numbers of protons and electrons. This deviation implies that the oxidation process of LEN involves an unequal proton-to-electron transfer, most likely proceeding via the participation of two electrons and one proton in the overall redox mechanism.

The electrochemical behavior of LEN is closely related to its ionization states, defined by its pK_a values (pK_{a1}≈2.3 and pK_{a2}≈11.5). Within the studied pH range, the molecule predominantly exists in its neutral form as the pH exceeds 2.14. The observed peak potential shift (–0.024V/pH) confirms that the oxidation is a proton-dependent process, where increasing the pH facilitates the loss of protons during the $2e^-/1H^+$ transfer mechanism. The optimal response at pH 4 suggests that the interaction between the neutral form of the analyte and the ZnFe-LDH@MnO_2 interface is maximized under these conditions.

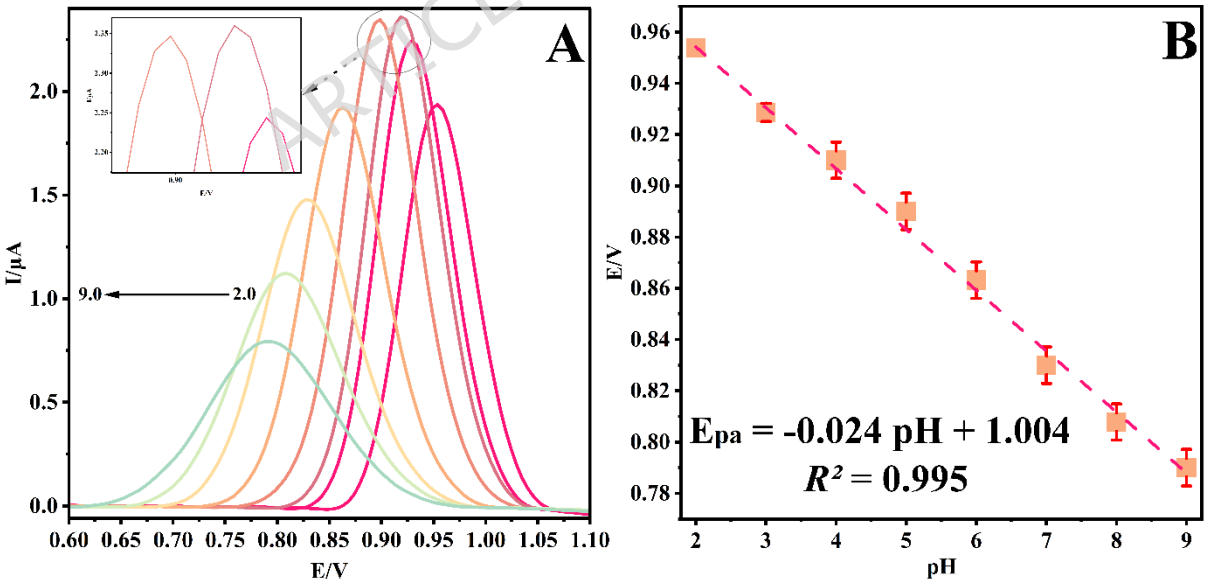


Figure 7. (A) DPV responses of 100 μM LEN on the ZnFe-LDH@MnO2/GCE in BR buffer at different pH values, and (B) the plot of peak position (Ip) versus pH for LEN.

Based on the proton-to-electron ratio obtained from the pH dependence studies, scan rate experiments were subsequently performed to further elucidate the number of electrons transferred and to gain insight

ARTICLE IN PRESS

into whether the oxidation process of LEN is diffusion- or adsorption-controlled. CV measurements were carried out at different scan rates ranging from 50 to 300 mV s^{-1}. As the scan rate increased, the oxidation peak current gradually increased and the peak potential shifted slightly toward more positive values, indicating a irreversible electrochemical process (Figure 8A). The plot of the oxidation peak current (I_p) versus the square root of the scan rate ($v^{1/2}$) exhibited a good linear relationship (R^2 = 0.991) with a slope of 0.067 (Figure 8B), suggesting that the oxidation of LEN is primarily diffusion-controlled. Furthermore, the linear correlation between log I_p and log v (R^2 = 0.096) with a slope of 0.379 and (Figure 8C) supports this conclusion. Additionally, the relationship between the peak potential (E_p) and the natural logarithm of the scan rate (ln v) yielded a slope of 0.022 (Figure 8D). Based on Laviron's equation, the number of electrons (n) involved in the electrooxidation of LEN was calculated to be approximately 2.33, indicating that the process involves the transfer of nearly two electrons, consistent with the proton–electron ratio obtained from the pH dependence studies.

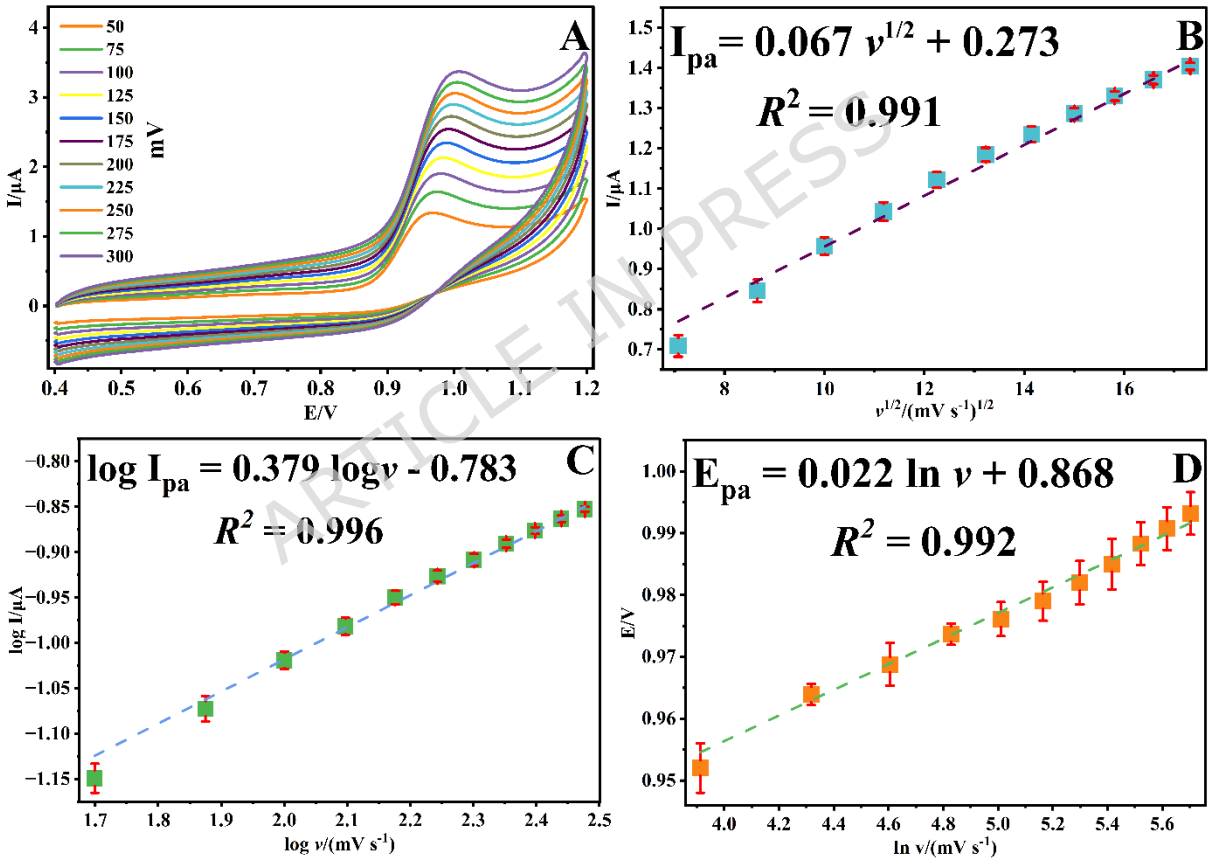
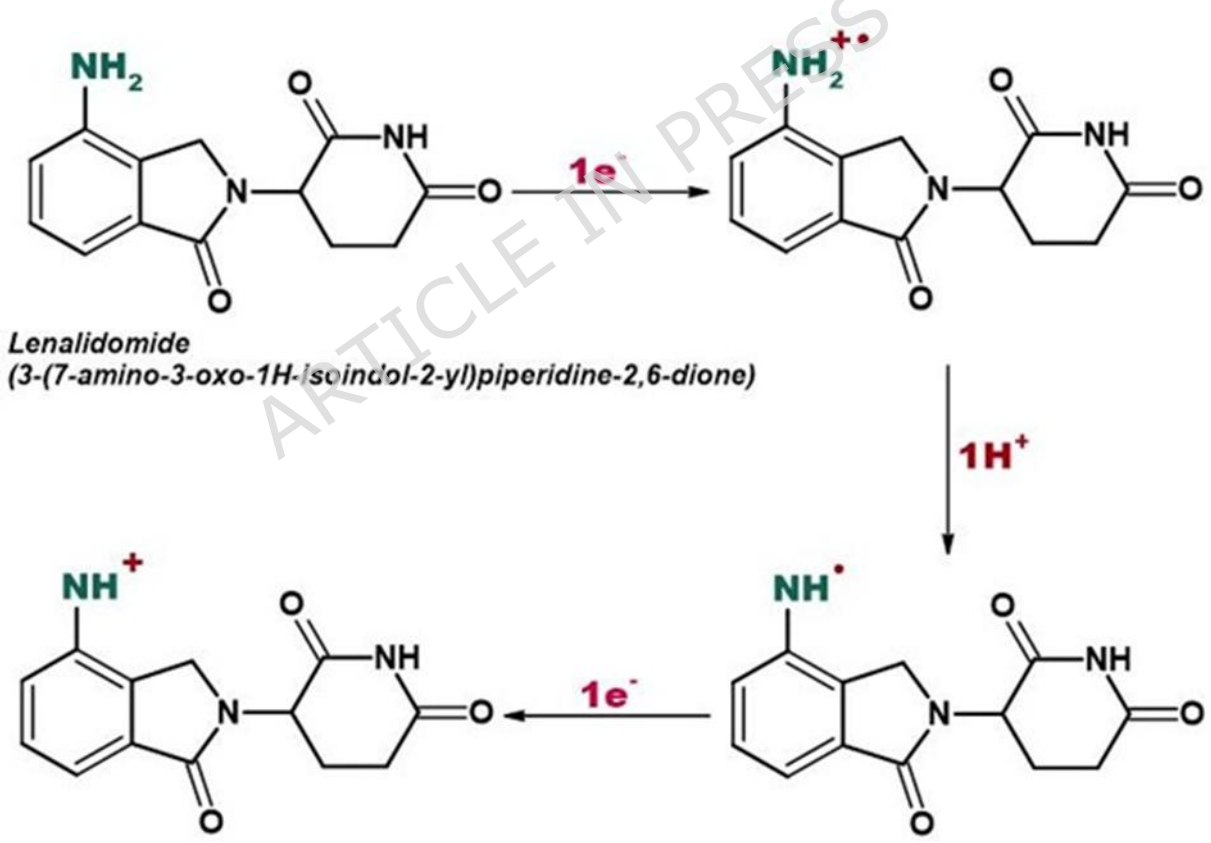


Figure 8. (A) CV curves recorded at scan rates ranging from 50 to 300 mV/s in BR buffer (pH 4.0) containing LEN (100 μM), (B) linear relationship between anodic peak current and the square root of the scan rate, (C) log–log plot of peak current versus scan rate, and (D) linear correlation between peak potential and the natural logarithm of the scan rate, all measured utilizing the ZnFe-LDH@MnO2/GCE.

ARTICLE IN PRESS

Based on the electrochemical data, which indicates an overall irreversible oxidation process involving the transfer of two electrons and one proton ($2e^-/1H^+$), a plausible mechanism for the electrooxidation of LEN is proposed.

The oxidation is suggested to initiate at the 4-amino group, as this aniline-like moiety represents the most electron-rich and easily oxidizable site within the molecule. In contrast, the other nitrogen and oxygen atoms are part of electron-deficient amide/imide and carbonyl groups, respectively, and are thus less susceptible to oxidation [50]. The mechanism is likely initiated by a one-electron ($1e^-$) transfer from the aromatic amino group to form a resonance-stabilized radical cation. This highly acidic intermediate then undergoes a rapid chemical step, consisting of a deprotonation to release one proton ($1H^+$) and form a neutral aminyl radical [51]. This radical species is more easily oxidized than the parent LEN molecule and immediately undergoes a second one-electron ($1e^-$) transfer. This final step generates a highly reactive nitrenium ion, or its corresponding quinone-imine derivative, which is likely responsible for the irreversible nature of the oxidation peak observed experimentally [52]. The suggested pathway is illustrated in Scheme 1.



Scheme 1. The proposed pathway for the electro-oxidation of LEN at ZnFe-LDH@MnO_2/GCE.

3.6. Analytical Performance

The variation of LEN peak currents with its concentration was investigated by means of the DPV technique, as illustrated in Figure 9A. To more clearly visualize the sensitivity and peak definition of

ARTICLE IN PRESS

the sensor at lower concentrations, the enlarged DPV responses for the initial concentration range are separately displayed in Figure 9B. The corresponding calibration plot including error bars is displayed in Figure 9C, demonstrating the reliability and precision of the obtained data. From these figures, it can be observed that the oxidation peak current increases linearly with rising LEN concentration within the range of 0.50–9.80 µM. Under optimized experimental parameters, the coefficient of determination was determined as 0.995 ($R^2 = 0.995$). The sensitivity of the developed ZnFe-LDH@MnO_2/GCE sensor was evaluated by determining the LOD and LOQ. These parameters were calculated according to the following equations:

$$LOD = \frac{3.3 \times \delta}{S}$$

$$LOQ = \frac{10 \times \delta}{S}$$

Where δ represents the standard deviation of the intercept (response) and S is the slope of the calibration plot [53]. Based on these calculations, the LOD and LOQ for LEN were found to be 6.99 nM and 23.31 nM, respectively.

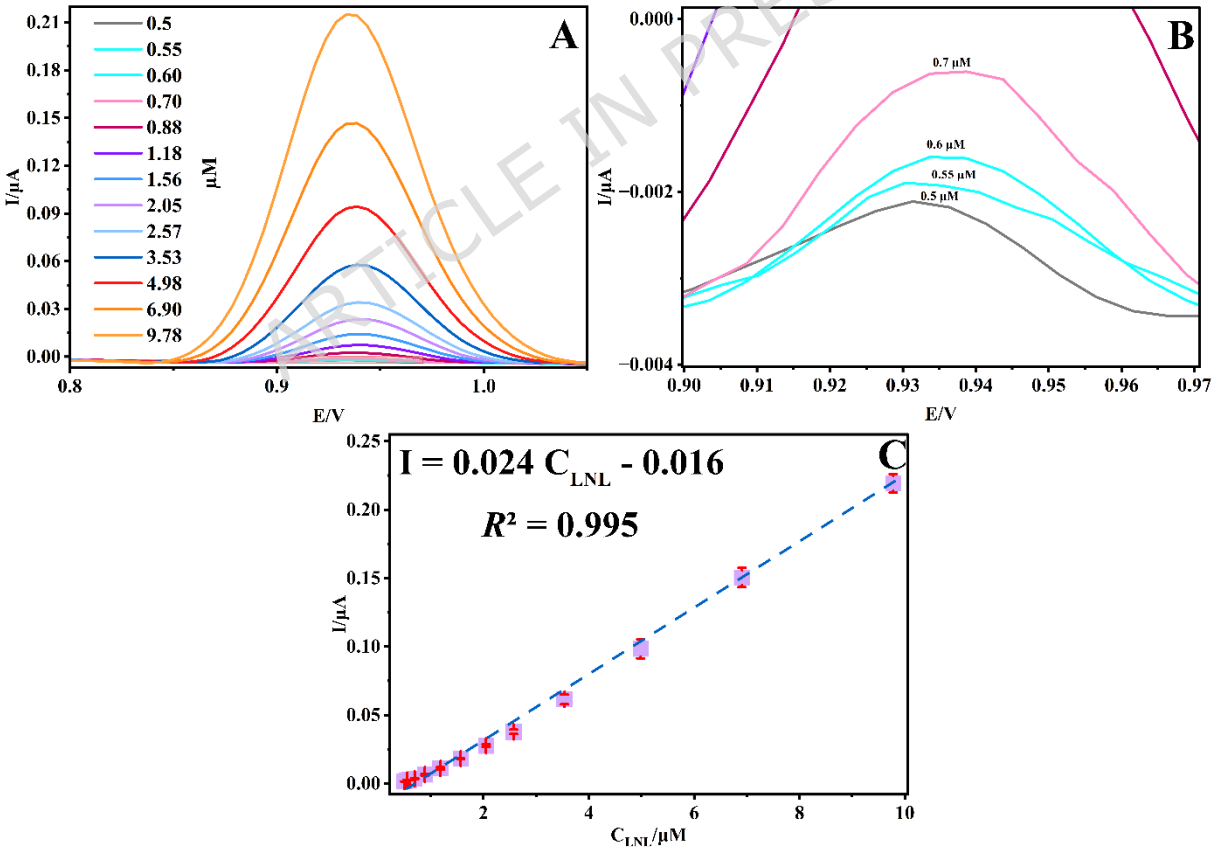


Figure 9. (A) DPV curves for varying concentrations of LEN, (B) enlarged DPV curves for lower concentrations, (C) calibration plot of peak current versus LEN concentration.

ARTICLE IN PRESS

To benchmark the analytical performance of the proposed ZnFe-LDH@MnO_2/GCE sensor, a comprehensive comparison with contemporary literature (2020–2026) was conducted, as summarized in Table 2. The developed sensor demonstrates a remarkably low LOD (6.99 nM), which is significantly superior to traditional UV-spectrophotometric and various HPLC-based methods reported to date. While complex chromatographic techniques provide high precision, our electroanalytical approach offers a more cost-effective, rapid, and 'greener' alternative by eliminating the need for organic solvents and expensive, bulky instrumentation. Furthermore, compared to highly sensitive but often expensive immunosensors (e.g., EIS-based platforms), the ZnFe-LDH@MnO_2 interface provides a much cheaper sensing environment with minimal preparation steps. The high recovery values obtained in human plasma, pharmaceutical formulations, and synthetic urine (98.2%–101.7%) are highly competitive with existing gold-standard protocols. These results underscore the exceptional robustness of the sensor in complex matrices and demonstrate that the proposed platform successfully bridges the gap between ultra-high sensitivity and practical sustainability for routine LEN determination.

Table 2. Comparison of the analytical performance of the developed ZnFe-LDH@MnO_2/GCE sensor with recent literature (2020–2026) for LEN determination.

Method	Linear Range	LOD	LOQ (or LLOQ)	Application	Recovery (%)	Ref
HPLC	5–30 µg/mL	0.30 µg/mL	1.00 µ/mL	Pharmaceutical formulation.	99.48–100.15	[54]
UV spectro.	5–30 µg/mL	0.70 µg/mL	2.10 µg/mL	Pharmaceutical formulation.	98.71–100.79	[54]
RP-HPLC	0.2-0.6 mg/mL	0.002-0.017 µg/mL	0.006- 0.056 µg/mL	LEN API form and its impurities.	92.4-109.7	[55]
RP-HPLC	0.112-1.875 ppm (Imp. A) 0.275-1.875 ppm (Imp. B)	0.0371 µg/mL (Imp. A) 0.1124 µg/mL (Imp. B)	0.0742 µg/mL (Imp. A) 0.2247 µg/mL (Imp. B)	LEN and its impurities.	98.5-109.6 (Imp. A) 98.3-104.9 (Imp. B)	[56]

ARTICLE IN PRESS

RP-HPLC	10-50 mcg/mL	1.1µg/mL	3.2µg/mL	LEN API form and its dosage form.	98.0-102	[57]
HPLC-UV	0.6-150 µg/L (water sample) 2.5-120 µg/L (plasma sample)	0.2–0.8 µg/L	0.6–2.5 µg/L	Water and plasma samples.	92.0-98.4	[58]
EIS	16 pg/ml-1 ng/ml	IKZF1: 0.68 pg/ml IKZF3: 0.97 pg/ml	-	Human serum.	92.6-101.2	[59]
DPV	**0.50–9.80 µM**	**6.99 nM**	**23.31 nM**	**Synthetic urine, human plasma, and pharmaceutical dosage form.**	**98.2-101.7**	**This work.**

ARTICLE IN PRESS

The precision of the proposed electrochemical method for the quantification of LEN was evaluated by assessing its repeatability and reproducibility. The repeatability, expressed as the RSD, was determined by performing consecutive measurements of LEN using a single ZnFe-LDH@MnO_2/GCE electrode. As shown in Figure S8A, the oxidation peak profiles corresponding to twelve sequential measurements of a 5 µM LEN solution are presented, while a magnified view of the peak apex region is provided in Figure S8B to better illustrate the signal consistency. The corresponding current–replicate diagram is displayed in Figure S8C, where the RSD was calculated as 1.1%.

Similarly, the reproducibility of the method was evaluated using ten independently fabricated ZnFe-LDH@MnO_2/GCE electrodes under optimized conditions. The associated voltammetric responses are given in Figure S8D, and the current–electrode diagram is shown in Figure S8E, yielding an RSD value of 0.4%. These results indicate good repeatability and reproducibility of the fabricated sensor in terms of both electrode preparation and voltammetric performance.

ARTICLE IN PRESS

The selectivity of the fabricated ZnFe-LDH@MnO_2/GCE sensor toward LEN detection was evaluated using 5 µM LEN in the presence of various potential interfering species. Inorganic salts such as potassium chloride, potassium nitrate, and sodium sulfate, as well as biological compounds including L-methionine, L-alanine, uric acid, and dopamine, were examined under identical experimental conditions. In addition, substances that may originate from pharmaceutical formulations or daily consumption, such as paracetamol and caffeine were also tested. To further address the sensor's discriminatory power, Pomalidomide (PML)—a structurally closely related thalidomide analog—was also examined as a challenging interferent. Remarkably, the introduction of Pomalidomide resulted in a negligible signal deviation of only 2.89%, even at a concentration significantly higher than that of the analyte.

The high selectivity observed can be attributed to the synergistic integration of the LDH matrix and MnO_2 nanostructures, which provides a high density of active redox sites that specifically facilitate the electron transfer of LEN. Notably, even for redox-active biological species like uric acid and dopamine, which often overlap with pharmaceutical signals, the proposed sensor maintained the integrity of the LEN oxidation peak without significant potential shifts. The corresponding voltammograms and the current–interferent diagram with error bars are presented in Figure S9A and Figure S9B, respectively. No significant variation in the LEN oxidation signal was observed in the presence of these substances, indicating acceptable selectivity of the sensor for LEN determination. The RSD was found to be 2.2%, further demonstrating that the ZnFe-LDH@MnO_2 interface effectively shields the electrode from non-specific adsorption and matrix-induced signal suppression. The quantitative effect of these species on the LEN peak current were calculated [60] and are summarized in Table S1, where all tested interferents resulted in signal deviations of less than 8.65%.

ARTICLE IN PRESS

3.7. Practical Applicability

To assess the practical applicability of the proposed method in real-world conditions, DPV measurements were performed in synthetic urine, human plasma, and pharmaceutical dosage form samples. For each concentration level, at least three replicate measurements were conducted, and the corresponding RSD and recovery values were calculated. As summarized in Table 3, the RSD values remained below 3.0%, not exceeding 1.3% in any case, indicating acceptable precision of the method in accordance with the acceptance criteria defined by ICH Q2(R1) [61]. Furthermore, the recovery values ranged between 98.2% and 101.7%, remaining within the 95–105% range recommended by the FDA and EMA guidelines for acceptable accuracy [62]. These findings indicate that the proposed electrochemical sensor can be reliably applied for LEN determination in complex biological and pharmaceutical matrices.

Table 3. Quantification of LEN in real sample types.

Sample	Added (µM)	Found (µM)	RSD%	Recovery

ARTICLE IN PRESS

Human Plasma	0.0	N.D.*	-	101.5
	2.0	2.03	0.5	98.2
	3.0	2.95	0.4	99.8
	5.0	4.99	1.3	
Synthetic Urine	0.0	N.D.*	-	98.9
	2.0	1.98	0.7	99.2
	3.0	2.98	0.6	101.7
	5.0	5.09	0.7	
Capsules	2.0	2.03	0.5	101.4
	3.0	2.99	0.7	99.6
	5.0	5.04	1.2	100.8

*N.D.: Not Detected.

3.8. Greenness Evaluation

The environmental impact and operational sustainability of the developed ZnFe-LDH@MnO_2/GCE sensor were comprehensively evaluated using three modern analytical assessment tools: GAPI, AGREE, and BAGI.

Initially, the GAPI was utilized to assess the qualitative greenness of the entire analytical life cycle, from sample collection and pretreatment to final waste disposal. This analysis highlighted the integration of eco-friendly solvent systems, such as ethanol–water mixtures, and the significant reduction in hazardous waste generation compared to conventional chromatographic methods [63]. The predominantly green and yellow color codes in the GAPI pictogram highlight the minimal sample preparation requirements, the use of eco-friendly solvent systems and the significant reduction in hazardous waste generation compared to conventional chromatographic methods (Figure 10A). Complementing this qualitative view, a quantitative evaluation was performed using the AGREE metric, which provides a weighted score based on the 12 principles of Green Analytical Chemistry. The method achieved a high score of 0.84 (Figure 10B), confirming its close alignment with these principles, particularly in terms of high sample throughput, energy-efficient operation, and the total elimination of toxic derivatization reagents [64].

Finally, the BAGI was employed to bridge the gap between sustainability and practical utility by measuring the "blueness" of the procedure. With a score of 77.5 (Figure 10C), the BAGI assessment underscores that the sensor is not only environmentally conscious but also robust and simple enough for routine application in complex pharmaceutical and biological matrices [65]. Collectively, these findings demonstrate that the ZnFe-LDH@MnO_2/GCE platform represents a green, efficient, and cost-effective alternative for the sensitive determination of LEN.

ARTICLE IN PRESS

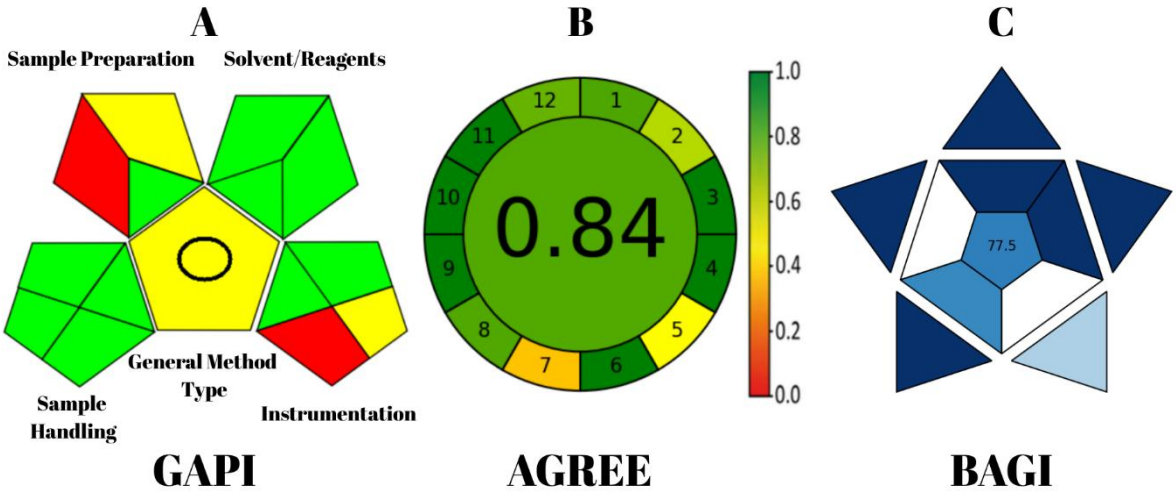


Figure 10. Comprehensive evaluation of the developed procedure's sustainability and applicability: (A) GAPI pictogram for qualitative greenness assessment; (B) AGREE analysis showing the quantitative greenness score of 0.84 ; and (C) BAGI index for practical utility assessment with a score of 77.5.

4. Conclusion

The ZnFe-LDH@MnO_2 nanocomposite-modified electrochemical sensor was successfully fabricated and applied for the sensitive voltammetric determination of LEN. Structural, morphological, and electrochemical analyses confirmed that MnO_2 decoration notably improved the conductivity, surface area, and electron-transfer efficiency of the ZnFe-LDH framework. Under optimized conditions, the sensor exhibited outstanding analytical performance, characterized by a linear concentration range of 0.50–9.80 µM, a LOD of 6.99 nM, and a LOQ of 23.31 nM. In addition, the platform demonstrated excellent precision, with repeatability (RSD = 1.1%) and reproducibility (RSD = 0.4%), as well as strong resistance to common interfering species. Its successful application to human plasma, synthetic urine, and pharmaceutical dosage forms—achieving recoveries between 98.2% and 101.7%—further confirms its practical applicability. Beyond its technical performance, the proposed method aligns with the principles of Green Analytical Chemistry, as evidenced by high GAPI, AGREE, and BAGI scores. The reduction in hazardous waste and the use of eco-friendly reagents make this platform a sustainable and environmentally conscious tool for clinical use. Owing to its simplicity, rapidity, low cost, and high sensitivity, the ZnFe-LDH@MnO_2/GCE sensor represents a promising and efficient alternative to chromatographic techniques for routine LEN quantification in biomedical and pharmaceutical settings.

Clinical trial number: not applicable.

Funding Declaration

This research did not receive any specific grant from funding agencies in the public, commercial, or not-for-profit sectors.

Data Availability

ARTICLE IN PRESS

Data will be available on request.

Ethics declarations

Ethics approval

No approval of research ethics committees was required to accomplish the goals of this study because synthetic materials were used in the experimental study.

Conflict of interest

The authors declare no competing interests.

Acknowledgements

This work was supported by the Scientific Research Project Office of Ankara University (A.Ü. BAP) (Project numbers: TSA-2025-3888 and TSA-2025-3852). In addition, this study was supported by the TÜBİTAK-BİDEB through the 2211–Domestic Graduate Scholarship Program. The author Ç. A. Özata is supported by the Scientific and Technological Research Council of Turkey (TÜBİTAK) under the 2211-A National PhD Scholarship Program.

References

1 Giannakoulas, N., Ntanasis-Stathopoulos, I. & Terpos, E. The role of marrow microenvironment in the growth and development of malignant plasma cells in multiple myeloma. *International journal of molecular sciences* **22**, 4462 (2021).

2 Raza, S., A Safyan, R. & Lentzsch, S. Immunomodulatory drugs (IMiDs) in multiple myeloma. *Current cancer drug targets* **17**, 846–857 (2017).

3 Rajkumar, S. V. *et al.* Combination therapy with lenalidomide plus dexamethasone (Rev/Dex) for newly diagnosed myeloma. *Blood* **106**, 4050–4053 (2005).

4 Lee, S. *et al.* Development and validation of an improved HPLC-MS/MS method for quantifying total and unbound lenalidomide in human plasma. *Pharmaceutics* **16**, 1340 (2024).

5 Iqbal, M., Wani, T. A., Khalil, N. Y. & Darwish, I. A. Development and validation of ultra-performance liquid chromatographic method with tandem mass spectrometry for determination of lenalidomide in rabbit and human plasma. *Chemistry Central Journal* **7**, 7 (2013).

6 Ranganathan, P., Gunasekaran, V., Singhvi, I. & Ansari, M. J. Development and validation of Lenalidomide in human plasma by LC-MS/MS. *Saudi journal of biological sciences* **26**, 1843–1847 (2019).

7 Neşetoğlu, N., Kaplan, C., Aslan, S. S. & Ünal, D. Ö. A simple and rapid LC-MS/MS method for therapeutic drug monitoring of lenalidomide. *Pakistan Journal of Analytical & Environmental Chemistry* **21**, 19–26 (2020).

8 Gopinath, R., Narenderan, S., Kumar, M. & Babu, B. Development and validation of a liquid chromatography-tandem mass spectrometric method for the determination of lenalidomide in human plasma and its application on bioequivalence studies. *Journal of Analytical Science and Technology* **10**, 33 (2019).

9 Darwish, I. A., Khalil, N. Y., Bakheit, A. H. & Alzoman, N. Z. A highly sensitive fluorimetric method for determination of lenalidomide in its bulk form and capsules via derivatization with fluorescamine. *Chemistry Central Journal* **6**, 118 (2012).

ARTICLE IN PRESS

10 Saxena, J., Saroj, S. & Rajput, S. Estimation of lenalidomide in bulk and its dosage form using uv spectrophotometric and Rp-Hplc methods. *Indo American journal of pharmaceutical research* **3**, 7938–7945 (2017).

11 Bharath, P., Gupta, P. S. & Ramachandran, D. Development and validation of stability indicating Rp-hplc method for quantitative estimation of lenalidomide in lenalidomide capsules dosage form. *Current Trends in Biotechnology and Pharmacy* **17**, 819–827 (2023).

12 Khalil, N. Y., Darwish, I. A., Wani, T. A. & Al-Majed, A.-R. A. Trace determination of lenalidomide in plasma by non-extractive HPLC procedures with fluorescence detection after pre-column derivatization with fluorescamine. *Chemistry Central Journal* **7**, 52 (2013).

13 Alshehrt, M., Maher, H., Alzoman, N., Sultan, M. & Darwish, I. STABILITY-INDICATING CAPILLARY ELECTROPHORESIS METHOD WITH PHOTODIODE ARRAY DETECTOR FOR DETERMINATION OF LENALIDOMIDE IN PHARMACEUTICAL PREPARATION. *Digest Journal of Nanomaterials & Biostructures (DJNB)* **8** (2013).

14 Öven, E. N., Genc, A. A., Erk, N., Ahmed, H. E. H. & Soylak, M. A novel NiCaAl-LDH@ ND-COOH nanocomposite-modified electrode for highly sensitive and selective electrochemical detection of larotrectinib in pharmaceutical and biological samples. *Microchimica Acta* **192**, 1–14 (2025).

15 Velraj, A., Alagarsamy, S. & Chen, S.-M. High-temperature assisted barium molybdate incorporation into heteroatom-doped porous carbon sheets for selective detection of sulfonamide derivatives. *Journal of Industrial and Engineering Chemistry* **142**, 707–715 (2025).

16 Abd-Elsabour, M. *et al.* A novel electrochemical sensor for detection of nicotine in tobacco products based on graphene oxide nanosheets conjugated with (1, 2-naphthoquinone-4-sulphonic acid) modified glassy carbon electrode. *Nanomaterials* **12**, 2354 (2022).

17 Alsoghier, H. M., Abd-Elsabour, M., Alhamzani, A. G., Abou-Krisha, M. M. & Assaf, H. F. Real samples sensitive dopamine sensor based on poly 1, 3-benzothiazol-2-yl ((4-carboxlicphenyl) hydrazono) acetonitrile on a glassy carbon electrode. *Scientific Reports* **14**, 16601 (2024).

18 Achache, M., El Boumlasy, S., Bouchta, D. & Choukairi, M. Development and applications of carbon paste and Sonogel-Carbon electrodes modified with nanomaterials: Perspectives in pharmaceutical, biological, environmental and food analysis: A review. *TrAC Trends in Analytical Chemistry*, 118502 (2025).

19 Velraj, A., Mariyappan, V., Shen-Ming, C. & Chen, Y.-S. Rare-Earth Perovskite-Supported Carbon Nanocomposite for Efficient Electrochemical Detection of Agricultural Pesticide Diphenylamine. *Journal of Environmental Chemical Engineering*, 120370 (2025).

20 Naser, M. *et al.* First electrochemical sensor for binimetinib based on graphene oxide–calcium molybdenum LDH: Fabrication, analytical performance, and Greenness assessment. *Electrochimica Acta*, 147016 (2025).

21 Mishra, G., Dash, B. & Pandey, S. Layered double hydroxides: A brief review from fundamentals to application as evolving biomaterials. *Applied Clay Science* **153**, 172–186 (2018).

22 Wang, Q. & O'Hare, D. Recent advances in the synthesis and application of layered double hydroxide (LDH) nanosheets. *Chemical reviews* **112**, 4124–4155 (2012).

23 Luo, J. *et al.* Layered double hydroxides for regenerative nanomedicine and tissue engineering: recent advances and future perspectives. *Journal of Nanobiotechnology* **23**, 370 (2025).

24 Zhou, A. *et al.* RSM-optimized Mg/Al-LDH biochar composite for enhanced phosphorus removal: Insights into interlayer structure evolution and adsorption mechanism. *Journal of Environmental Management* **401**, 128837 (2026).

25 Zhang, Y. *et al.* Cysteine-Intercalated ZnFe-LDH as an Enhanced Peroxidase Nanozyme via Valence Regulation for Efficient Antibacterial Therapy. *ACS Applied Bio Materials* (2026).

ARTICLE IN PRESS

26 Saeed, M. *et al.* Visible-light-active Zn–Fe Layered Double Hydroxide (LDH) for the photocatalytic conversion of rice husk extract to value-added products. *Applied Sciences* **12**, 2313 (2022).

27 Gong, M. *et al.* An advanced Ni–Fe layered double hydroxide electrocatalyst for water oxidation. *Journal of the American Chemical Society* **135**, 8452–8455 (2013).

28 Toupin, M., Brousse, T. & Bélanger, D. Charge storage mechanism of MnO2 electrode used in aqueous electrochemical capacitor. *Chemistry of Materials* **16**, 3184–3190 (2004).

29 Li, Z. *et al.* Determination of Mn valence states in nanocatalysts during sustainable syngas conversion. *Journal of the American Chemical Society* **147**, 32548–32559 (2025).

30 Nie, Y. *et al.* Metal organic framework coated MnO2 nanosheets delivering doxorubicin and self-activated DNAzyme for chemo-gene combinatorial treatment of cancer. *International journal of pharmaceutics* **585**, 119513 (2020).

31 Shahparast, S. & Asadpour-Zeynali, K. α-MnO2/FeCo-LDH on nickel foam as an efficient electrocatalyst for water oxidation. *ACS omega* **8**, 1702–1709 (2022).

32 Liu, W., Xu, W., Dong, G. & Fang, M. Controlled Fabrication of Hierarchically Structured MnO2@ NiCo-LDH Nanoarrays for Efficient Electrocatalytic Urea Oxidization. *Nanomaterials* **13**, 2268 (2023).

33 Elshishini, H. M., Elsubruiti, G. M., Ghatass, Z. F. & Eltaweil, A. S. Microwave-assisted synthesis of Zn–Fe LDH modified with magnetic oxidized hydrochar for Pb (II) removal: insights into stability, performance and mechanism. *Journal of Solid State Chemistry* **335**, 124689 (2024).

34 Polson, C., Sarkar, P., Incledon, B., Raguvaran, V. & Grant, R. Optimization of protein precipitation based upon effectiveness of protein removal and ionization effect in liquid chromatography–tandem mass spectrometry. *Journal of Chromatography B* **785**, 263–275 (2003).

35 Sarigul, N., Korkmaz, F. & Kurultak, İ. A new artificial urine protocol to better imitate human urine. *Scientific reports* **9**, 20159 (2019).

36 He, C. *et al.* Waste shrimp shell-derived hydrochar as an emergent material for methyl orange removal in aqueous solutions. *Environment international* **134**, 105340 (2020).

37 Arain, M. B. & Soylak, M. Synthesis of magnetic multi-walled carbon nanotubes with layered double hydroxide (M-MWCNTs@ MnAl-LDH) nanocomposite as an adsorbent for lead extraction. *Food Chemistry* **463**, 141311 (2025).

38 Yadav, D. K., Uma, S. & Nagarajan, R. Microwave-assisted synthesis of ternary Li-M-Al LDHs (M= Mg, Co, Ni, Cu, Zn, and Cd) and examining their use in phenol oxidation. *Applied Clay Science* **228**, 106655 (2022).

39 Zaher, A., Taha, M., Farghali, A. A. & Mahmoud, R. K. Zn/Fe LDH as a clay-like adsorbent for the removal of oxytetracycline from water: combining experimental results and molecular simulations to understand the removal mechanism. *Environmental Science and Pollution Research* **27**, 12256–12269 (2020).

40 Yang, F. *et al.* Assembling biochar with various layered double hydroxides for enhancement of phosphorus recovery. *Journal of hazardous materials* **365**, 665–673 (2019).

41 Zheng, W., Sun, S., Xu, Y., Yu, R. & Li, H. Facile synthesis of NiAl-LDH/MnO2 and NiFe-LDH/MnO2 composites for high-performance asymmetric supercapacitors. *Journal of Alloys and Compounds* **768**, 240–248 (2018).

42 Wang, Y., Sun, H., Ang, H. M., Tadé, M. O. & Wang, S. Facile synthesis of hierarchically structured magnetic MnO2/ZnFe2O4 hybrid materials and their performance in heterogeneous activation of peroxymonosulfate. *ACS applied materials & interfaces* **6**, 19914–19923 (2014).

43 Soylak, M., Oguz, F. & Ahmed, H. E. H. CoNiFe-LDH nanoflowers combined with bismuth-based layered perovskite oxide (Bi_2MoO_6) for vortex-assisted micro-solid phase extraction of lead from food and water samples. *Food Chemistry*, 145177 (2025).

ARTICLE IN PRESS

44 Huang, C., Tang, C., Wu, Q. & Zhu, Q. Magnetic MnFe2O4/ZnFe-LDH for enhanced phosphate and Cr (VI) removal from water. *Environmental Science and Pollution Research* **29**, 59224–59234 (2022).

45 Wang, J., Li, S., Guo, Y., Ding, J. & Lu, Z. Preparation of S-Doped Ni-Mn-Fe Layered Hydroxide for High-Performance of Oxygen Evolution Reaction. *Coatings* **15**, 825 (2025).

46 Özata, Ç. A. *et al.* Electrochemical detection of riociguat using COF-PTA@ CuCoFe-LDH modified glassy carbon electrode: A novel approach for pharmaceutical and biological analysis. *Microchemical Journal* **211**, 113158 (2025).

47 Tan, Q. *et al.* In situ construction of ZnFe-layered double oxides on biochar for improving interfacial adsorption-catalysis of ozone achieves efficient water purification. *Separation and Purification Technology*, 135358 (2025).

48 Meléndez-Marmolejo, J. *et al.* Design and application of molecularly imprinted polymers for adsorption and environmental assessment of anti-inflammatory drugs in wastewater samples. *Environmental Science and Pollution Research* **29**, 45885–45902 (2022).

49 Tu, J., Cai, W. & Shao, X. Direct quantitative analysis from the current curve data of pulse voltammetric techniques. *Journal of Electroanalytical Chemistry* **725**, 25–31 (2014).

50 Nateghi, M. *et al.* Autoacceleration/degradation of electrochemical polymerization of substituted anilines. *Polymer* **46**, 11476–11483 (2005).

51 Eberson, L. in *Advances in physical organic chemistry* Vol. 18 79–185 (Elsevier, 1982).

52 Falvey, D. E. Nitrenium ions. *Reactive intermediate chemistry*, 593–650 (2003).

53 Velraj, A. *et al.* Fruitful design of novel SrV2O6@ MCM-41-based electrochemical sensor for carcinogenic carbendazim detection in complex real-world matrices. *Composites Part B: Engineering* **300**, 112475 (2025).

54 Demir, İ., Bulduk, İ. & Enginar, H. Development, validation and greenness assessment of environmentally friendly analytical methods for the quantification of lenalidomide in pharmaceutical formulations. *Acta Chromatographica* **36**, 395–405 (2024).

55 Cao, Z. *et al.* Simultaneous determination of thirteen related substances in lenalidomide API by a stability-indicating RP-HPLC method. *Journal of Pharmaceutical and Biomedical Analysis* **260**, 116823 (2025).

56 Sitamahalakshmi, D., Bharath, P., Ramachandran, D. & Ramamurty, D. Stability Indicating RP-HPLC Method for Quantitative Estimation of Lenalidomide and Its Impurities in Solid Dosage Form.(2023). *Int. J. Life Sci. Pharma Res* **13**, P29–P42.

57 SWATHI, K. *et al.* METHOD DEVELOPMENT AND VALIDATION FOR THE QUANTITATIVE ESTIMATION OF LENALIDOMIDE IN API FORM AND MARKETED TABLET DOSAGE FORM BY RP-HPLC. *Journal For Innovative Development in Pharmaceutical and Technical Science (JIDPTS)* **7** (2024).

58 Movahedi, F., Ezoddin, M., Adlnasab, L. & Shojaei, R. Magnetic Graphene Oxide Modified with a Surface-Active Ionic Liquid for Ultrasound-Assisted Solid-Phase Extraction (UA-SPE) to Preconcentrate Lenalidomide from Human Plasma with Determination by High-Performance Liquid Chromatography with Ultraviolet Detection (HPLC-UV). *Analytical Letters* **56**, 1685–1700 (2023).

59 Abdulkarim, H., Zourob, M. & Siaj, M. Development of label-free impedimetric immunosensors for IKZF1 and IKZF3 femtomolar detection for monitoring multiple myeloma patients treated with lenalidomide. *Scientific Reports* **10**, 10424 (2020).

60 Achache, M., Bouchta, D., Draoui, K. & Choukairi, M. Low-cost electrochemical sensor based on montmorillonite for the simultaneous detection of phenolic pollutants in tap and bottled water. *Journal of Environmental Chemical Engineering* **13**, 115981 (2025).

61 Borman, P. & Elder, D. Q2 (R1) validation of analytical procedures: text and methodology. *ICH quality guidelines: an implementation guide*, 127–166 (2017).

62 Fda, U. Bioanalytical method validation guidance for industry. *US Department of Health and Human Services Food and Drug Administration Center for Drug Evaluation and Research and Center for Veterinary Medicine* (2018).

ARTICLE IN PRESS

63 Abdelrahman, M. M. in *Green chemical analysis and sample preparations: Procedures, instrumentation, data metrics, and sustainability* 29–99 (Springer, 2022).

64 Imam, M. S. & Abdelrahman, M. M. How environmentally friendly is the analytical process? A paradigm overview of ten greenness assessment metric approaches for analytical methods. *Trends in Environmental Analytical Chemistry* **38**, e00202 (2023).

65 Hammad, S. F., Hamid, M. A. A., Adly, L. & Elagamy, S. H. Comprehensive review of greenness, whiteness, and blueness assessments of analytical methods. *Green Analytical Chemistry* **12**, 100209 (2025).

ARTICLE IN PRESS